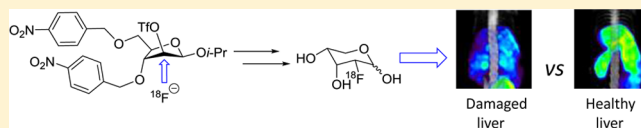


Development of 2-Deoxy-2-[¹⁸F]fluororibose for Positron Emission Tomography Imaging Liver Function in VivoNikolai M. Evdokimov,^{*,†,§,●} Peter M. Clark,^{‡,●} Graciela Flores,^{§,||} Timothy Chai,[‡] Kym F. Faull,^{⊥,#} Michael E. Phelps,^{§,||} Owen N. Witte,^{‡,§,∞,○} and Michael E. Jung^{*,†,§}[†]Department of Chemistry and Biochemistry, University of California, Los Angeles, California 90095, United States[‡]Department of Microbiology, Immunology, and Molecular Genetics, [§]Department of Molecular and Medical Pharmacology, ^{||}Crump Institute for Molecular Imaging, [⊥]Psychiatry and Biobehavioral Sciences, [#]Pasarow Mass Spectrometry Laboratory, Semel Institute for Neuroscience and Human Behavior, [∞]Eli and Edythe Broad Center of Regenerative Medicine and Stem Cell Research, and [○]Howard Hughes Medical Institute, David Geffen School of Medicine, University of California, Los Angeles, California 90095, United States

S Supporting Information

ABSTRACT: Life-threatening acute liver failure can be triggered by a variety of factors, including common drugs such as acetaminophen. Positron emission tomography (PET) is rarely used to monitor liver function, in part because of a lack of specific imaging agents for liver function. Here we report a new PET probe, 2-deoxy-2-[¹⁸F]fluororibose ([¹⁸F]-2-DFR), for use in imaging liver function. [¹⁸F]-2-DFR was synthesized and validated as a competitive substrate for the ribose salvage pathway. [¹⁸F]-2-DFR was prepared through an efficient late stage radiofluorination. The desired selectivity of fluorination was achieved using an unorthodox protecting group on the precursor, which could withstand harsh S_N2 reaction conditions with no side reactions. [¹⁸F]-2-DFR accumulated preferentially in the liver and was metabolized by the same enzymes as ribose. [¹⁸F]-2-DFR could distinguish between healthy liver and liver damaged by acetaminophen. [¹⁸F]-2-DFR is expected to be a useful PET probe for imaging and quantifying liver functions in vivo, with likely significant clinical utility.



■ INTRODUCTION

Positron emission tomography (PET) is a clinically relevant imaging modality for quantitatively measuring biochemical pathways in vivo.^{1,2} PET images the selective accumulation of radiolabeled imaging probes in specific cell populations due to unique metabolic or protein expression profiles targeted by the probes. PET is used both preclinically and clinically to study in vivo metabolism, to provide a molecular imaging diagnostic of the biology of disease, to aid in drug discovery and development, and to stratify patient populations for drug trials and treatments.^{1–4} Historically, carbohydrate-based PET probes have played a central role in the use of PET.^{1,2} The fluorinated glucose analogue 2-deoxy-2-[¹⁸F]fluoroglucose ([¹⁸F]-FDG) has for decades been used as a tool clinically to investigate alterations in glycolysis in normal and diseased states of the brain and heart and to detect, stage, and assess therapeutic efficacy in cancer patients.^{1–6}

The liver is a vital organ responsible for a remarkable plethora of biological functions, including detoxifying blood, producing albumin, and maintaining blood glucose levels. A variety of blood tests exists that provide systemic assessments of liver function.^{7–9} Imaging modalities such as ultrasound and magnetic resonance imaging have been used but suffer from limited resolution and specificity in the case of ultrasound.⁸ The PET imaging probe [¹⁸F]-FDG does not accumulate significantly in the liver.² Liver biopsies are invasive, associated with a risk of complications, and suffer from limited tissue

sampling.¹⁰ Noninvasive, quantitative methods for imaging local changes in specific biological functions of the liver are lacking. Yet in many cases, quantifying the extent of liver damage and injury remains a significant clinical challenge and can lead to unnecessary and expensive clinical interventions.¹¹ This led to our interest in developing PET probes to image specific biochemical pathways in the liver. An early study showed that [³H]-ribose, injected into rats intravenously, accumulates in hepatocytes, and recently it was demonstrated that [¹⁴C]-ribose, injected into mice intravenously, accumulates preferentially in the liver through the activity of the ribose salvage pathway.^{12,13} This suggested that molecules that measure the activity of the ribose salvage pathway in vivo could be scaffolds upon which to build clinically useful hepatic PET probes.

The synthesis of PET probes is often difficult because of the short half-life of the ¹⁸F radionuclide (109.8 min) and a limited set of available efficient and selective methods with which to introduce ¹⁸F into molecules.¹⁴ In most cases, this requires that ¹⁸F be installed at or near the last step in the synthesis in a reaction that produces no fluorinated side products. Any subsequent deprotection step must be fast, high yielding, and preferably devoid of side products.

Received: April 11, 2015

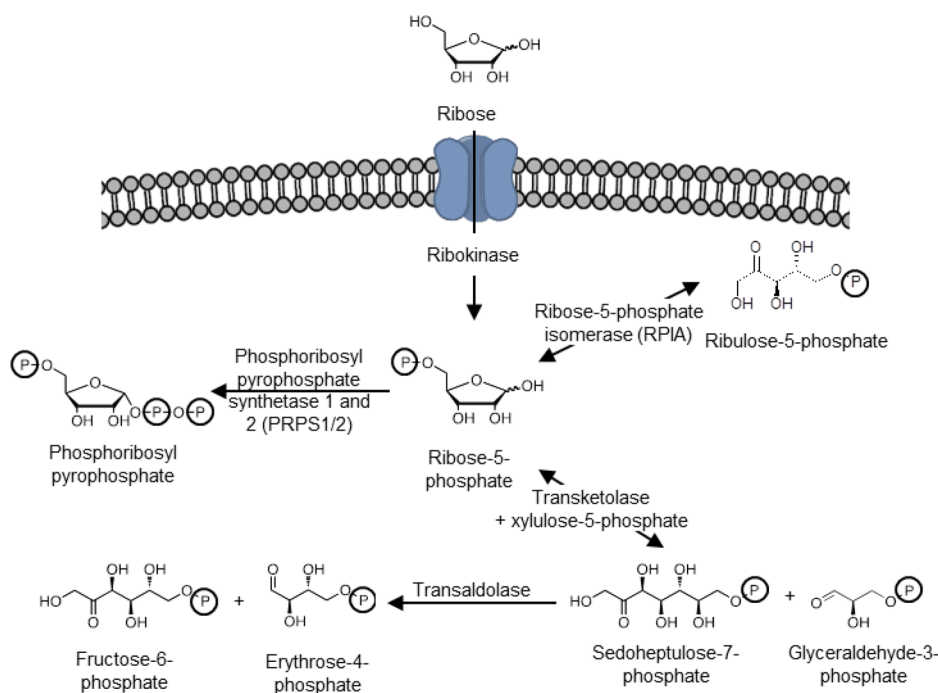
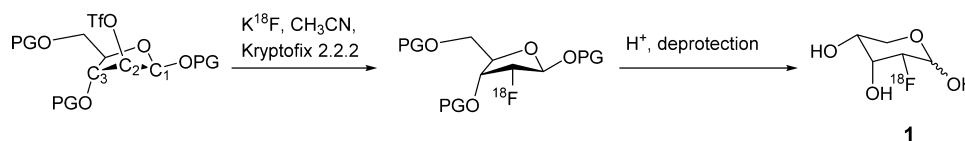


Figure 1. Ribose salvage and metabolism pathways.

Scheme 1. Proposed Synthesis of [^{18}F]-2-DFR (1)



We recently developed and evaluated an ^{18}F fluorinated ribose derivative, 2-deoxy-2- ^{18}F fluoroarabinose (^{18}F -DFA), as a PET imaging probe to measure the ribose salvage pathway.¹² When injected intravenous into mice, [^{18}F]-DFA accumulates strongly and selectively in the liver.¹² However, upon further analysis, we identified that mice injected with [^{18}F]-DFA and imaged with PET showed significant accumulation of radioactivity in bone tissue that increased over the course of an hour (Figure S1, Supporting Information). Mice injected with [^{14}C]-ribose and imaged by autoradiography after an hour of accumulation failed to show any significant signal enrichment in bone tissue (Figure S1, Supporting Information). This strongly suggests that [^{18}F]-DFA is defluorinated in vivo. The undesired presence of radioactivity in bone tissue would mask any specific accumulation of the probe in the bone marrow, and hepatic probe defluorination could complicate image quantification, particularly in the liver. There is a need for an alternative PET imaging probe for measuring the ribose salvage pathway. Recently the PET imaging probe 5-deoxy-5- ^{18}F fluororibose has been described.^{15,16} 5-Deoxy-5-fluororibose replaces the 5-hydroxyl of ribose with a fluorine, a modification that blocks phosphorylation of this probe by the ribose kinase ribokinase, the first enzyme in the ribose salvage pathway (Figure 1).¹⁷ The inability of ribokinase to phosphorylate 5-deoxy-5-fluororibose limits the utility of 5-deoxy-5- ^{18}F fluororibose as a probe to measure the ribose salvage pathway in vivo. Thus, we decided to pursue the synthesis of a new ribose-based PET probe.

DFA differs from ribose both in the replacement of the 2-hydroxyl with a fluorine atom and by epimerization at this

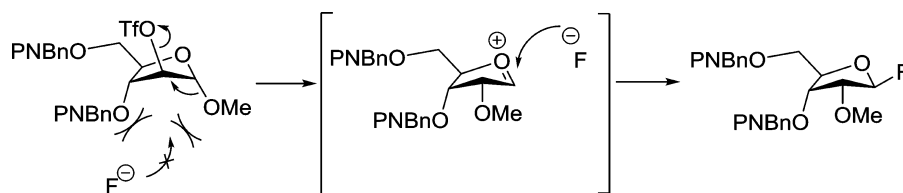
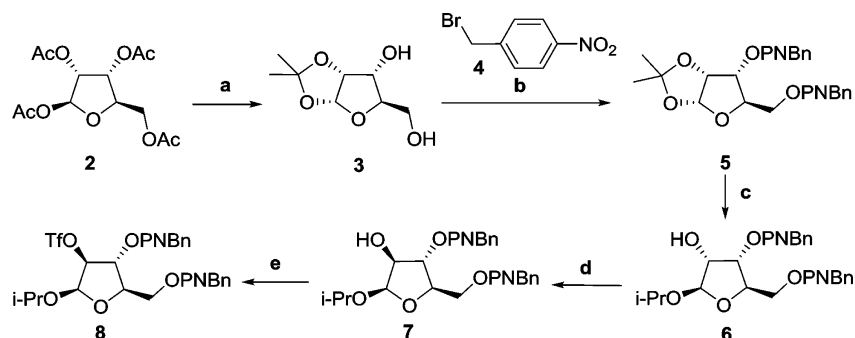
stereocenter. 2-Deoxy-2-fluororibose (2-DFR) differs from ribose only in the replacement of the 2-hydroxyl with a fluorine atom and is stereochemically identical to ribose. We pursued the synthesis and evaluation of [^{18}F]-2-DFR with the goal of developing a PET imaging probe that would be an improvement over DFA and 5-deoxy-5-fluororibose in simultaneously being able to measure ribose salvage activity while being resistant to defluorination in vivo.

RESULTS AND DISCUSSION

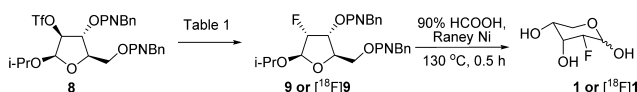
Chemical Synthesis. Although modern synthetic chemistry offers a range of methods to introduce ^{18}F into molecules,^{14,18–20} undoubtedly the stereoselective labeling of an aliphatic carbon in a carbohydrate is best performed using a rapid $\text{S}_{\text{N}}2$ reaction on a carefully designed precursor. We envisioned achieving the synthesis of [^{18}F]-2-DFR (1) by performing an $\text{S}_{\text{N}}2$ reaction on a protected arabinose bearing a good leaving group, such as triflate, at C-2 (Scheme 1).

This seemingly trivial synthetic task was complicated by the fact that the C-3 hydroxyl protecting group hinders the C-2 position from attack by the incoming fluoride. A more serious concern was possible anchimeric assistance from ether or ester protecting groups at C-3 that would stabilize a carbocation at C-2 and possibly even lead to rearrangements. The same would be true for protecting groups on the C-1 hydroxyl. After exploring several synthetic avenues, we realized that an electron deficient protecting group had to be installed on the hydroxyl group at C-3.

Scheme 2. Possible Mechanism for Side Product Formation

Scheme 3. Synthesis of Precursor 8 for Radiofluorination^a

^a(a) (i) cat. I₂, acetone, rt, 4 h, (ii) NaOMe, MeOH, 50 °C, 30 min, 83% (2 steps); (b) 4, Ag₂O, CH₂Cl₂, 40 °C, 20 h, 87%; (c) (i) cat. TfOH, Ac₂O, AcOH, rt, 3 h, (ii) cat. I₂, *i*-PrOH, THF, 67 °C, 8 h, (iii) NaOMe, MeOH, rt, 15 min, 64% (3 steps); (d) (COCl)₂, DMSO, Et₃N, CH₂Cl₂, -78 °C to rt, 40 min, (ii) NaBH₄, H₂O, EtOH, 0 °C, 15 min, 87% (two steps); (e) Tf₂O, pyridine, CH₂Cl₂, 0 °C, 30 min, 96%.

Table 1. Optimization of the Synthesis of 1 and [¹⁸F]-1

number	reagent (equiv)	solvent	time (min)	temp (°C)	yield of 9 or [¹⁸ F]-9 (%)
1	KF (1.0), K222 (1.0)	DMF	20	160	dec
2	KF (1.0), K222 (1.0)	DMF	40	120	5
3	TBAF (1.0)	<i>t</i> -BuOH	50	120	33
4	KF (1.0), K222 (1.0)	MeCN	50	120	57
5	KF (1.0), K222 (1.0)	MeCN	50	120, MW	72
6	KF (1.0), K222 (1.0)	MeCN	30	154 ^a	76
7	K[¹⁸ F], K222	MeCN	45	154 ^a	84 ^b
8	K[¹⁸ F], K222	MeCN	30	154 ^a	78 ± 5 ^{b,c}
9	K[¹⁸ F], K222	MeCN	30	154 ^d	34
10	K[¹⁸ F], K222	MeCN	10	154 ^a	41 ^b

^aIn house radiosynthesizer, sealed vessel, 10 mg of precursor. ^bDecay corrected yield. ^c*n* = 10. ^d5 mg of precursor.

Formation of C-1 fluoride (Scheme 2) was eliminated by utilizing the pure β -anomeric precursor. Thus, the arabinofuranoside **8**, with PNBn protecting groups at the C-3 and C-5 position, was synthesized (Scheme 3). This sequence involved the two-step formation of the α -acetonide **3** from **2** followed by protection of the diol as the bis(4-nitrobenzyl) ether **5**.²¹ Next, the 1,2-acetonide protection in **5** was converted to the 1,2-*O*-diacetate, and selective formation of the 1- β -isopropoxy acetal, with the help of the C-2 α -acetate group providing anchimeric assistance, followed by saponification, finally gave the α -alcohol **6**. Inversion of the 2-alcohol via oxidation–reduction, and final triflate formation afforded the substrate **8** in 40% overall yield. The bulky β -isopropoxy group at the anomeric position was chosen to increase the *anti* delivery of hydride during the hydride reduction, allowing a more efficient overall inversion and higher yield of compound **7**. The [¹⁹F] NMR spectrum of the product **9** displayed the expected peak at –209 ppm for a fluorine atom at C-2, which was previously observed by the

Woerpel group,²² while the NMR of compound C-1 fluorides shows a peak at –116 ppm.²³

Fluorination of the triflate **8** was examined under several conditions (Table 1), and it was found that clean formation of the protected fluororibose **9** was accomplished in 72% yield after 50 min of heating in acetonitrile at 120 °C using microwave irradiation and 76% yield after 30 min of heating in acetonitrile under sealed conditions at 154 °C. The global deprotection of **9** was achieved quantitatively by treatment with Raney Ni at 130 °C in formic acid for 30 min, producing 2-DFR (**1**) as the expected mixture of mostly the α,β -pyranose anomers.²⁴

Radiofluorination was best performed at 154 °C in acetonitrile for 30 min under sealed conditions using 10 mg of triflate **8** and gave 78 ± 5% conversion with no detectable side product, as determined by radio-TLC (Table 1, entry 8; Figure 2a). Lower temperatures, shorter incubation times, and lower amounts of precursor all decreased the fluorination

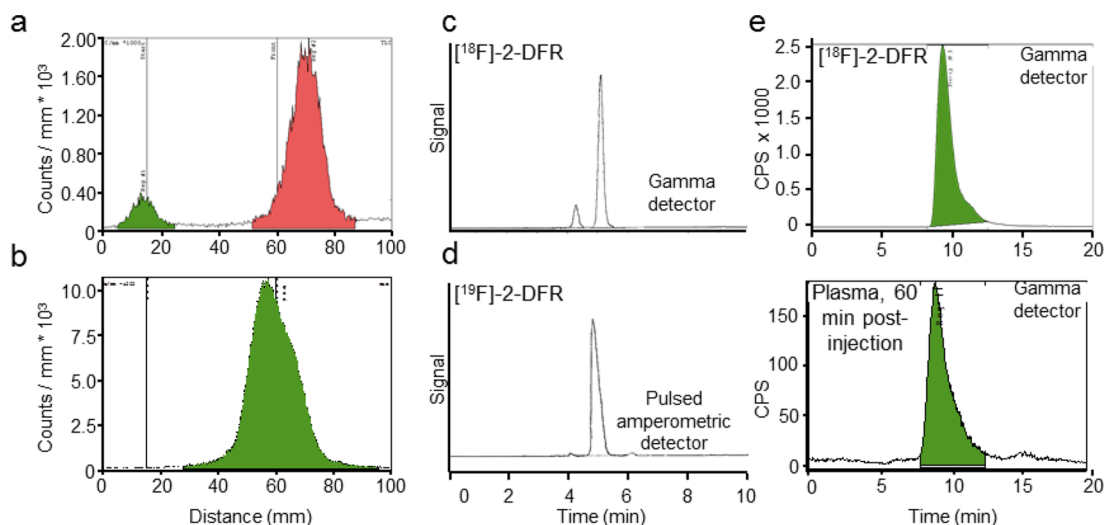


Figure 2. $[^{18}\text{F}]$ -2-DFR is an isotopologue of $[^{19}\text{F}]$ -2-DFR and is stable in vivo. (a) Radio-TLC of the radiolabeling reaction mixture. Red peak: $[^{18}\text{F}]$ -9. Green peak: $^{18}\text{F}^-$. (b) Radio-TLC of the deprotection of $[^{18}\text{F}]$ -9. Green peak: $[^{18}\text{F}]$ -1. (c) $[^{18}\text{F}]$ -2-DFR and (d) $[^{19}\text{F}]$ -2-DFR were analyzed by high performance anion exchange chromatography connected to a pulsed amperometric detector and a γ detector. (e) $[^{18}\text{F}]$ -2-DFR was injected into mice, and after 60 min, the mouse plasma was analyzed by an HPLC connected to a γ detector and compared with pure $[^{18}\text{F}]$ -2-DFR.

efficiency (Table 1). $[^{18}\text{F}]$ -9 was purified by a silica gel cartridge and subsequently deprotected with Raney Ni in formic acid in $70 \pm 5\%$ yield at 130°C for 30 min, as determined by radio-TLC (Figure 2b). The PET tracer **1** was produced in a total synthetic time of 150 min (from $[^{18}\text{F}]$ -fluoride delivery to formulation) with a final decay-corrected radiochemical yield of $12 \pm 2\%$. The $[^{18}\text{F}]$ -2-DFR radiochemical purity was $95 \pm 3\%$, as measured by high performance anion exchange chromatography in combination with a pulsed amperometric detector and a γ detector, with the predominant impurity eluting at the same retention time as $[^{18}\text{F}]$ -DFA (Figure 2c).¹² To confirm the fidelity of the $[^{18}\text{F}]$ -2-DFR synthesis, $[^{18}\text{F}]$ -2-DFR and $[^{19}\text{F}]$ -2-DFR were injected into the same system. $[^{18}\text{F}]$ -2-DFR eluted at the same time as the $[^{19}\text{F}]$ -2-DFR standard (Figure 2c,d), suggesting that $[^{18}\text{F}]$ -2-DFR was correctly prepared and represents an ^{18}F -fluorinated isotopologue of $[^{19}\text{F}]$ -2-DFR. Finally the specific activity of $[^{18}\text{F}]$ -2-DFR was determined to be 74 ± 30.9 TBq/mmol. These analyses collectively suggest that $[^{18}\text{F}]$ -2-DFR is suitable for PET imaging experiments.

Biological Analysis. The main motivation behind the development of $[^{18}\text{F}]$ -2-DFR was to identify a PET imaging probe that measures the ribose salvage pathway but that is resistant to defluorination in vivo. To assess the stability of $[^{18}\text{F}]$ -2-DFR in vivo, $[^{18}\text{F}]$ -2-DFR was injected into mice and, after an hour, their serum was analyzed using an HPLC connected to a γ detector. The HPLC chromatograms from the plasma of the injected mice were nearly identical to the HPLC chromatogram of pure $[^{18}\text{F}]$ -2-DFR with no additional peaks or shifts in retention time (Figure 2e). This suggests that 2-DFR is stable in vivo for up to 60 min and provides early evidence that 2-DFR is not subject to defluorination.

Mice intravenously injected with $[^{18}\text{F}]$ -2-DFR showed high uptake in the liver and kidneys, with additional uptake in the intestines, as measured and quantified by PET imaging, time activity curves, and ex vivo biodistribution studies (Figure 3a–c; ex vivo biodistribution values: liver, $11.38 \pm 1.74\%$ injected dose/gram (% ID/g); kidney, $11.14 \pm 1.59\%$ ID/g; intestines, $7.37 \pm 1.07\%$ ID/g). $[^{18}\text{F}]$ -2-DFR accumulated in the liver within 15 min and remained there for at least 2 h (Figure 3c). Notably radioactivity was largely absent from the bone, and the

amount of radioactivity in the bone was stable for at least 2 h (Figure 3a,c). Except for the difference in bone uptake, the whole body biodistribution of $[^{18}\text{F}]$ -2-DFR is qualitatively and quantitatively similar to the whole body biodistribution of $[^{18}\text{F}]$ -DFA and $[^{14}\text{C}]$ -ribose (Figure S2, Supporting Information).¹² Whole body autoradiography of a mouse intravenously injected with $[^{18}\text{F}]$ -2-DFR and imaged after 1 h of accumulation showed uniform and strong labeling throughout the liver with additional signal in the kidney and intestines, consistent with the PET imaging (Figure 3d). No significant accumulation of radioactivity was present in the bones. Previously we identified that hepatocytes salvage ribose at a much higher rate than Kupffer, stellate, or endothelial cells.¹² The strong, uniform $[^{18}\text{F}]$ -2-DFR accumulation in the liver is consistent with $[^{18}\text{F}]$ -2-DFR accumulation in liver hepatocytes. Additionally THLE-2 cells, an immortalized human hepatocyte cell line, accumulated $[^{18}\text{F}]$ -2-DFR through a pathway that could be blocked with excess ribose (Figure 3e). To determine whether $[^{18}\text{F}]$ -2-DFR accumulated in the liver through the same pathway as ribose, a competition experiment was performed. Co-injection of $[^{18}\text{F}]$ -2-DFR with ribose significantly decreased hepatic and intestinal $[^{18}\text{F}]$ -2-DFR accumulation but failed to change renal $[^{18}\text{F}]$ -2-DFR accumulation (Figure 3f), suggesting that hepatic and intestinal $[^{18}\text{F}]$ -2-DFR signal is due to specific accumulation. Collectively our data suggest that $[^{18}\text{F}]$ -2-DFR is a PET imaging probe that measures ribose salvage activity, that $[^{18}\text{F}]$ -2-DFR is not subject to defluorination in vivo, and that $[^{18}\text{F}]$ -2-DFR accumulates significantly in hepatocytes in vivo.

To better understand how 2-DFR is transformed inside cells and to add further evidence that 2-DFR measures ribose salvage activity, we studied its metabolism using cell culture and in vitro enzymatic assays. During salvage, the glucose transporter Slc2a2 and likely other proteins transport extracellular ribose into cells where ribokinase phosphorylates ribose to ribose-5-phosphate (Figure 1).^{12,17} In cell culture experiments, phosphorylated 2-DFR levels were (9.1 ± 0.7) -fold higher in 293T cells that overexpressed Slc2a2 and ribokinase than in 293T cells that overexpressed ribokinase alone (Figure 4a), suggesting that 2-DFR is a substrate for Slc2a2 and additionally that 2-DFR is

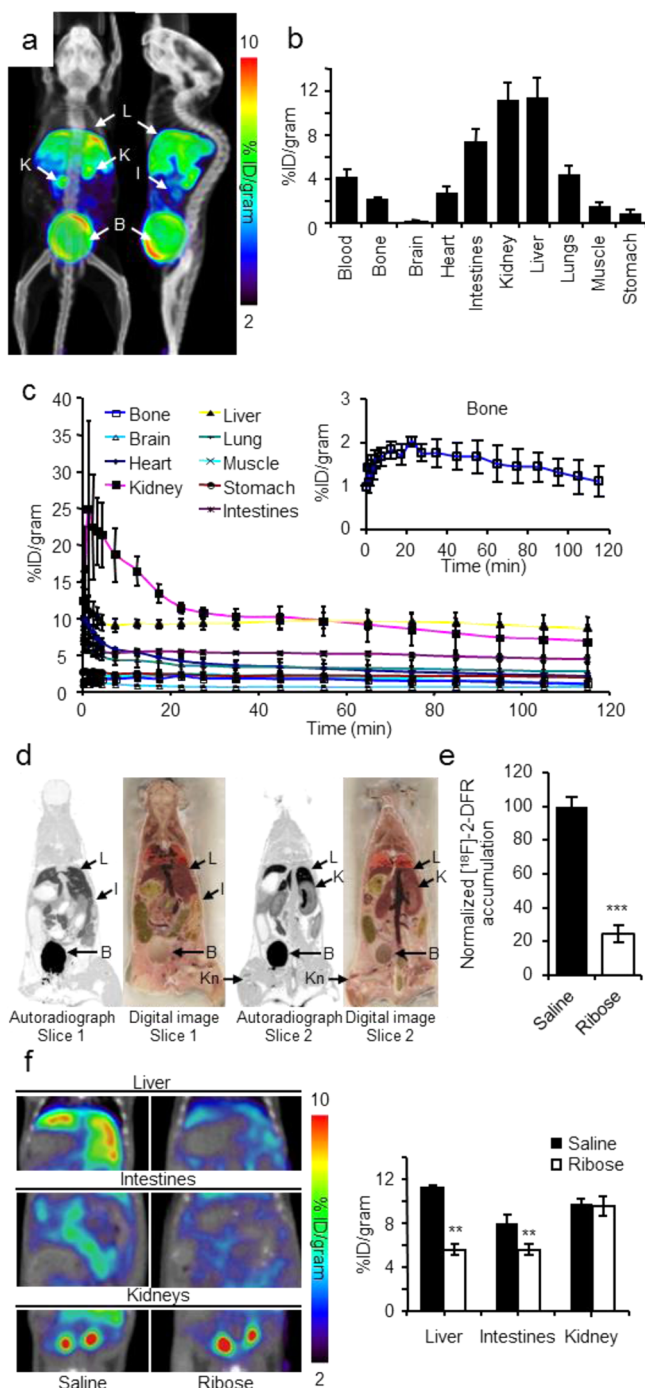


Figure 3. $[^{18}\text{F}]-2\text{-DFR}$ strongly accumulates in the liver and kidney in vivo. (a) PET/CT image of a mouse intravenously injected with $[^{18}\text{F}]-2\text{-DFR}$ and imaged for 10 min, 1 h later, after which a 10 min CT scan was performed. % ID/gram = percent injected dose per gram of tissue; L = liver, K = kidney, I = intestines, B = bladder. (b) Ex vivo biodistribution of $[^{18}\text{F}]-2\text{-DFR}$. (c) Time–activity curves of $[^{18}\text{F}]-2\text{-DFR}$ accumulation in several organs from immediate postinjection to 2 h postinjection. (d) Whole body autoradiography of a mouse intravenously injected with $[^{18}\text{F}]-2\text{-DFR}$ following 1 h of accumulation. L = liver, K = kidney, I = intestines, B = bladder, Kn = Knee. (e) $[^{18}\text{F}]-2\text{-DFR}$ accumulation in a hepatocyte-like cell line in the presence of saline or excess ribose. (f) PET/CT images and quantification of mice intravenously injected with $[^{18}\text{F}]-2\text{-DFR}$ and saline or ribose. (**) $P < 0.01$; (***) $P < 0.001$.

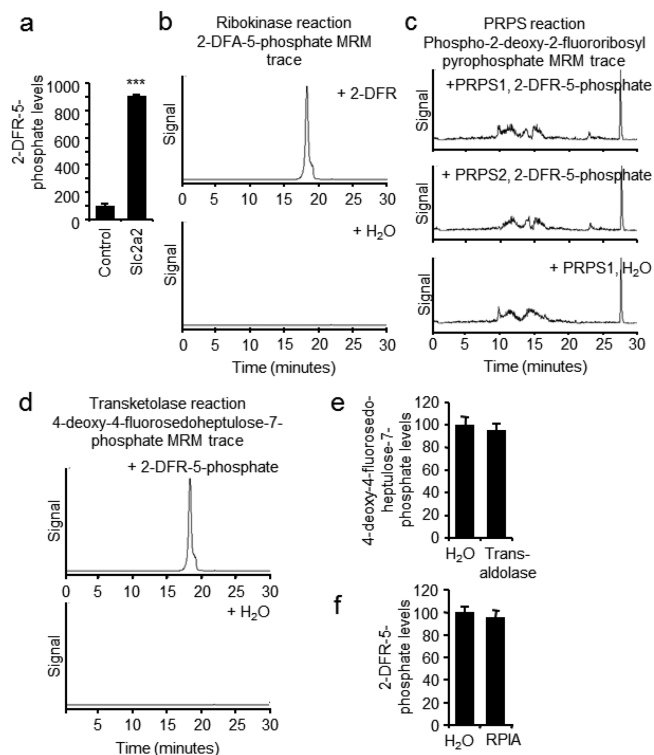


Figure 4. 2-DFR is transported into cells by the glucose transporter Slc2a2, phosphorylated by ribokinase, and further metabolized by the enzyme transketolase. (a) 2-DFR-5-phosphate levels in cells that overexpress ribokinase (control) or ribokinase and Slc2a2 (Slc2a2). (b) 2-DFR-5-phosphate MRM trace of an in vitro reaction containing ribokinase and 2-DFR or H₂O. (c) Phospho-2-deoxy-2-fluororibosyl pyrophosphate MRM trace of an in vitro reaction containing PRPS1 or PRPS2 and 2-DFR-5-phosphate or H₂O. (d) 4-Deoxy-4-fluorosedoheptulose-7-phosphate MRM trace of an in vitro reaction containing transketolase and 2-DFR-5-phosphate or H₂O. (e) 4-Deoxy-4-fluorosedoheptulose-7-phosphate levels in an in vitro reaction containing 4-deoxy-4-fluorosedoheptulose-7-phosphate and transaldolase or H₂O. (f) 2-DFR-5-phosphate levels in an in vitro reaction containing 2-DFR-5-phosphate and RPIA or H₂O. (***) $P < 0.001$.

phosphorylated in cells, potentially by ribokinase. To determine whether 2-DFR is a substrate for ribokinase, bacterially expressed human ribokinase was combined with ribose, 2-DFR, or vehicle (H₂O) in vitro and the reaction products were identified by LC/MS/MS-MRM. Ribokinase phosphorylated ribose to ribose-5-phosphate and 2-DFR to 2-DFR-5-phosphate (Figure 4b; Figure S3, Supporting Information). Ribokinase has a K_m of 3.5×10^{-5} M (standard error, 2.5×10^{-5} M) and a V_{max} of 2.6×10^{-11} molecules of 2-DFR-5-phosphate $s^{-1} \mu g^{-1}$ for 2-DFR compared to a K_m of 6.9×10^{-5} M (standard error, 1.3×10^{-5} M) and a V_{max} of 8.2×10^{-11} ribose-5-phosphate $s^{-1} \mu g^{-1}$ for ribose. Thus, 2-DFR is an effective substrate for ribokinase with greater affinity but slower kinetics than the endogenous substrate ribose.

In cells, ribose-5-phosphate is used in the de novo nucleotide synthesis pathway or is metabolized through the nonoxidative pentose phosphate pathway. The first enzymes that metabolize ribose-5-phosphate for de novo nucleotide synthesis are phosphoribosyl pyrophosphate synthetase 1 and 2 (PRPS1 and PRPS2). The first enzymes that metabolize ribose-5-phosphate through the nonoxidative pentose phosphate pathway are ribose-5-phosphate isomerase (RPIA) and the sequential enzymes transketolase and transaldolase. RPIA

isomerizes ribose-5-phosphate to ribulose-5-phosphate while transketolase and transaldolase convert ribose-5-phosphate and the related pentose xylulose-5-phosphate first to sedoheptulose-7-phosphate and glyceraldehyde-3-phosphate and then to fructose-6-phosphate and erythrose-4-phosphate (Figure 1).²⁵

Human PRPS1, PRPS2, transketolase, transaldolase, and RPIA were expressed and isolated from bacteria and were active against their natural substrates (Figure S3, Supporting Information). PRPS1 and PRPS2 failed to metabolize 2-DFR-5-phosphate (Figure 4c). Transketolase metabolized 2-DFR-5-phosphate to 4-deoxy-4-fluorosedoheptulose-7-phosphate, but transaldolase failed to further metabolize 4-deoxy-4-fluorosedoheptulose-7-phosphate (Figure 4d, e). Similarly RPIA failed to metabolize 2-DFR-5-phosphate (Figure 4f). This suggests that 2-DFR is metabolized by ribokinase and transketolase, at which point it cannot be further metabolized.

Finally, we assessed whether [¹⁸F]-2-DFR could be used to study and image changes in liver function. Acetaminophen overdose is the leading cause of acute liver failure in the developed world, and treatment often requires a liver transplant.^{11,26,27} Distinguishing between individuals who require a liver transplant and those who will recover without a transplant remains a significant clinical challenge.¹¹

Mice treated with a high dose of acetaminophen (300 mg/kg) or saline control had significantly elevated blood levels of the liver enzymes alanine aminotransferase and aspartate aminotransferase 5 h after treatment (Figure 5a). At the same

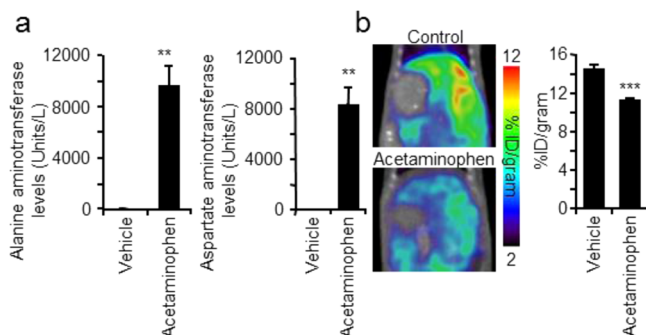


Figure 5. [¹⁸F]-2-DFR can be used to study acetaminophen toxicity, a model of liver failure. (a) Alanine aminotransferase and aspartate aminotransferase levels in mice treated with vehicle or acetaminophen. (b) [¹⁸F]-2-DFR PET/CT image and quantification of mice treated with vehicle or acetaminophen. All experiments were performed three independent times. (**) $P < 0.01$; (***) $P < 0.001$.

time point, mice treated with acetaminophen showed a decrease in [¹⁸F]-2-DFR accumulation from $14.5 \pm 0.4\%$ ID/g to $11.3 \pm 0.2\%$ ID/g (Figure 5b), which could be caused by a variety of mechanisms, including down-regulation of the ribose salvage pathway, fewer hepatocytes, and decreased blood perfusion. Future studies will be required to determine this mechanism in detail. Additional studies will also have to be performed to determine whether the change in signal during acetaminophen toxicity is greater than the natural variation of hepatic [¹⁸F]-2-DFR signal in patients. However, these studies provide initial data to suggest that [¹⁸F]-2-DFR may be a useful tool for studying and diagnosing acetaminophen toxicity preclinically and clinically.

CONCLUSIONS

We have described the synthesis and validation of a novel PET probe, [¹⁸F]-2-DFR, for quantifying ribose salvage activity in vivo. [¹⁸F]-2-DFR was synthesized in 12% radiochemical yield and 74 ± 30.9 TBq/mmol specific activity from precursor 8. [¹⁸F]-2-DFR contains an unusual cis-oriented ¹⁸F and hydroxyl group and was challenging to synthesize because of the threat of poor stereoselectivity during the fluorination step caused by anchimeric assistance of nearby oxygen lone pair electrons. This anchimeric assistance was completely suppressed by utilizing a pure β -anomeric precursor, which allowed efficient stereospecific late stage fluorination in a short period of time, a requirement for the synthesis of PET imaging tracers. 2-DFR is a fluorinated ribose analogue that acts as a competitive substrate with ribose for the Slc2a2 protein transporter and ribokinase and transketolase enzymes. The accumulation of 2-DFR and its metabolites is proportional to the activity of the ribose salvage pathway, which can be examined in vivo with PET using [¹⁸F]-2-DFR. Unlike the previously described [¹⁸F]-DFA PET imaging probe, [¹⁸F]-2-DFR is not subject to defluorination in vivo. A model of liver dysfunction from a high dose of acetaminophen in mice was used to demonstrate that PET imaging with [¹⁸F]-2-DFR provided an in vivo measure of liver dysfunction in a clinically relevant model of hepatotoxicity. Collectively, the data provide evidence that [¹⁸F]-2-DFR is a novel PET probe that can be used to study and quantify ribose salvage in vivo in experimental models and potentially patients.

EXPERIMENTAL SECTION

Chemical Procedures. All reagents and catalysts were purchased from commercial sources (Acros Organics and Sigma-Aldrich) and used without purification unless otherwise noted. Ethanol (200 proof) was purchased from the UCLA Chemistry Department (Los Angeles, CA, USA). Hydrochloric acid (1 N) and polypropylene filters (0.45 μ m) were purchased from Fisher Scientific. tC18 (WAT036810), silica (WAT020520 and WAT043400), alumina (WAT020505), and Accell plus QMA (quarternary methylammonium; WAT020545) cartridges were purchased from Waters. Cartridges for trapping and releasing ¹⁸F (MPI) were purchased from Ortg, Inc. (Oakdale TN). AG50 strong cation exchange and AG11 ion retardation resins were purchased from Biorad. The KT-500-2 column set was purchased from Isoflex. The QMA cartridges were preconditioned with KHCO₃ (5 mL; 1 M) and washed with water (10 mL) followed by K₂CO₃ (0.4 mL; 0.605 M) and air (10 cc). The tC18 cartridges were preconditioned with EtOH (5 mL) followed by water (10 mL). The silica cartridges were preconditioned with anhydrous hexane (6 mL). Alumina cartridges were preconditioned with H₂O (10 mL). AG50 and AG11 resins were manually packed into small cartridges and preconditioned with water. All reactions were performed under inert atmosphere of dry argon and monitored by thin layer chromatography (TLC) on precoated (250 μ m) silica gel 60F254 glass-backed plates or on EMD silica gel 60 F254 TLC aluminum sheets and visualized with a UV-254 lamp or 10% sulfuric acid in ethanol stain. NMR spectra were obtained on Bruker AV300 and AV500 instruments at the UCLA MIC Magnetic Resonance Laboratory. DART-MS spectra were collected on a Thermo Exactive Plus MSD (Thermo Scientific) equipped with an ID-CUBE ion source and a Vapur Interface (IonSense). Both the source and MSD were controlled by Excalibur, version 3.0. The analyte was spotted onto OpenSpot sampling cards (IonSense) using methanol as the solvent. Ionization was accomplished using He plasma with no additional ionization agents. Flash column chromatography was performed on silica gel (32–63 μ m, 60 Å pore size). Chemical shifts (δ) are reported in ppm relative to the TMS internal standard. Abbreviations are as follows: s (singlet), d (doublet), t (triplet), q (quartet), m (multiplet).

1,2-O-Isopropylidene-D-ribofuranose (3). To a solution of 3.05 g (9.6 mmol) of 1,2,3,5-tetra-*O*-acetyl- β -D-ribofuranose (**2**) in 30 mL of dry (4 Å molecular sieves for 10 h) acetone was added 0.6 g (2.4 mmol) of elemental iodine, and the reaction was stirred under argon at room temperature for 4 h. Dichloromethane (100 mL) was added, and the reaction was washed with NaHCO₃ (20 mL of sat. aq solution) followed by Na₂S₂O₃ (20 mL of 10% aq solution). The aqueous fractions were extracted with 2 × 30 mL of dichloromethane. The combined organic fractions were washed with 50 mL of brine, dried with Na₂SO₄, and the solvent was removed via rotary evaporation. The vacuum-dried crude material was dissolved in 30 mL of dry MeOH, and 0.4 g of NaOMe was added to the solution. The reaction was stirred for 30 min at 50 °C. Once TLC (4% MeOH in CH₂Cl₂) showed a single spot with *R*_f = 0.34, Amberlyst-15 resin was added to neutralize the reaction. The resin beads were removed by filtration, and mother liquor was concentrated via rotary evaporation. Upon careful removal of solvent, the crude material was sufficiently pure for use in the next step. Purification by column chromatography on silica gel eluting with MeOH/CH₂Cl₂ (0–4% gradient) afforded 1.51 g (83%) of **3** as a clear oil crystallizing with time. The spectroscopic data were in agreement with that in the literature.²⁸

1,2-O-Isopropylidene-3,5-di-O-(4-nitrobenzyl)-D-ribofuranose (5). The diol **3** (1.5 g, 7.89 mmol) was coevaporated with 10 mL of toluene and mixed with 10 g (43 mmol) of Ag₂O and 10 g of activated 4 Å molecular sieves (150 °C for 3 d). The solids were suspended in dry dichloromethane (80 mL) and stirred for 1 h. Then 6.5 g (28 mmol) of 4-nitrobenzyl bromide was added in one portion and the reaction was stirred at 40 °C under argon for 20 h. The reaction was filtered through Celite, rinsed with 3 × 15 mL of dichloromethane and the solvent dried in vacuo. Silica gel column chromatography using EtOAc/hexanes (15–35% gradient) provided 3.2 g (87%) of pure compound **5** (*R*_f = 0.28, 35% of EtOAc in hexanes, HPLC *t*_R = 6.20 min). **5**: ¹H NMR (500 MHz, CDCl₃) δ 8.19 (dd, *J* = 8.5 Hz, 2H), 8.18 (d, *J* = 8.5 Hz, 2H), 7.53 (d, *J* = 8.5 Hz, 2H), 7.46 (d, *J* = 8.5 Hz, 2H), 5.82 (d, *J* = 3.5 Hz, 1H), 4.88 (d, *J* = 13.0 Hz, 1H), 4.70–4.63 (m, 4H), 4.25 (ddd, *J* = 9.0, 4.0, 2.0 Hz, 1H), 3.89 (dd, *J* = 9.0, 4.5 Hz, 1H), 3.86 (dd, *J* = 11.5, 2.0 Hz, 1H), 3.71 (dd, *J* = 11.5, 4.5 Hz, 1H), 1.60 (s, 3H), 1.38 (s, 3H). ¹³C NMR (125 MHz, CDCl₃) δ 147.9, 147.7, 145.9, 145.4, 128.3, 127.9, 124.0, 123.9, 113.5, 104.6, 78.5, 78.2, 77.2, 72.6, 71.2, 69.2, 27.0, 26.9. MS (TOF ES⁺) *m/z* calcd C₂₂H₂₈N₃O₉ [M + NH₄⁺], 478.18255; found, 478.17804.

Isopropyl 3,5-Di-O-(4-nitrobenzyl)-β-D-ribofuranoside (6). To an ice-cold solution of the acetone **5** (3.16 g, 6.85 mmol) in a mixture of acetic acid (36 mL) and acetic anhydride (9 mL), 0.03 mL (0.34 mmol) of TfOH was added, and reaction was kept at room temperature for 3 h. The reaction was carefully neutralized with NaOH (1 M), and mixture of acetates (EtOAc/hexanes = 1/2; *R*_f = 0.27 β-anomer; *R*_f = 0.23 α-anomer) was extracted with dichloromethane (3 × 75 mL). The organic phases were combined and dried over Na₂SO₄, and the solvent was removed via rotary evaporation. The crude material was dissolved in 15 mL of dry THF. To that solution were added iodine (0.35 g, 1.39 mmol) and dry isopropanol (2 mL, 27 mmol), and the reaction was refluxed under argon for 8 h. The solvent was removed by rotary evaporation and the residue dissolved in 100 mL of dichloromethane. The solution was washed with NaHCO₃ (20 mL saturated aqueous solution) followed by Na₂S₂O₃ (20 mL of 10% aqueous solution), and the organic layer was dried over Na₂SO₄ and reduced in vacuo. TLC (1% MeOH in CH₂Cl₂) indicated two major spots with *R*_f = 0.54 (isopropyl 2-*O*-acetyl-3,5-di-*O*-PNBn-β-D-ribofuranoside) and **6** with *R*_f = 0.12. The crude material was dissolved in 30 mL of dry MeOH, and 0.2 g of NaOMe was added. The reaction was stirred for 30 min at 50 °C. TLC (EtOAc/hexanes = 1/2) showed one spot with *R*_f = 0.18. Amberlyst-15 resin was added to the reaction. The resin beads were removed by filtration, and the solvent was removed using rotary evaporation. The crude material was chromatographed on silica gel, eluting with a gradient of 20–40% of EtOAc in hexanes to afford 2.02 g of **6** (HPLC *t*_R = 9.97). **6**: ¹H NMR (300 MHz, CDCl₃) δ 8.21 (d, *J* = 8.7 Hz, 2H), 8.20 (d, *J* = 8.7 Hz, 2H), 7.51 (dd, *J* = 9.0 Hz, 2H), 7.48 (d, *J* = 9.0 Hz, 2H), 5.11 (s, 1H), 4.78 (d, *J* = 12.9 Hz, 1H), 4.71 (d, *J* = 12.9 Hz, 1H), 4.69 (s, 2H), 4.29

(ddd, *J* = 5.7, 5.7, 5.7 Hz, 1H), 4.15 (ddd, *J* = 4.8, 4.8, 4.8 Hz, 1H), 4.12 (s, 1H), 3.94 (septet, *J* = 6.0 Hz, 1H), 3.66 (dd, *J* = 11.4, 4.9 Hz, 1H), 3.65 (dd, *J* = 11.6, 5.7 Hz, 1H), 2.54 (d, *J* = 3.6 Hz, 1H), 1.14 (d, *J* = 6.3 Hz, 3H), 1.12 (s, *J* = 6.3 Hz, 3H). ¹³C NMR (125 MHz, CDCl₃) δ 148.0, 147.8, 145.9, 144.8, 128.1, 127.9, 124.1, 124.0, 105.9, 80.8, 80.2, 77.6, 74.0, 72.9, 72.4, 71.7, 69.9, 23.8, 21.7. MS (TOF ES⁺) *m/z* calcd C₂₂H₃₀N₃O₉ [M + NH₄⁺], 480.19820; found, 480.19355.

Isopropyl 3,5-Di-O-(4-nitrobenzyl)-β-D-arabinofuranoside (7). To a solution of oxalyl dichloride (1.07 mL, 12.5) in 20 mL of dichloromethane was added dropwise a solution of DMSO (1.73 mL, 24.3 mmol) in 5 mL of dichloromethane at –78 °C. After the mixture was stirred for 15 min, a solution of the ribofuranoside (**6**) (1.9 g, 4.1 mmol) in 25 mL of dichloromethane was added. After the mixture was stirred at –78 °C for 40 min, Et₃N (3.4 mL, 24.7 mmol) was added. The solution was warmed to room temperature over 5 min, mixed with H₂O (50 mL), and extracted with dichloromethane (50 mL twice). TLC (EtOAc/hexanes = 1/2) showed one spot with *R*_f = 0.26. The organic phase was dried with Na₂SO₄ and concentrated. The crude material was dissolved in 20 mL of EtOH–CH₂Cl₂ (8:2) mixture, and NaBH₄ (0.31 g, 8.1 mmol) dissolved in 13 mL of EtOH–H₂O (2:1) was added dropwise with stirring at 0 °C. The reaction was then warmed to ambient temperature over 1 h and quenched with 10% AcOH. The mixture was extracted from NaHCO₃ (aq sat. solution 100 mL) with 2 × 100 mL of dichloromethane. The combined organic layer was washed with 2 × 100 mL of water and then dried over Na₂SO₄. The solvent was removed under vacuum. TLC displayed compound **7** with *R*_f = 0.21 (EtOAc/hexanes = 1/2) and a hardly visible spot of compound **6** with *R*_f = 0.18, HPLC *t*_R = 6.61. Column chromatography of the residue on silica gel (30–40% of EtOAc in hexanes) afforded 1.64 g (87%) of **7**: ¹H NMR (500 MHz, CDCl₃) δ 8.21 (d, *J* = 8.8, 2H), 8.19 (d, *J* = 8.8 Hz, 2H), 7.51 (d, *J* = 8.8 Hz, 2H), 7.50 (d, *J* = 8.8 Hz, 2H), 5.11 (d, *J* = 4.9 Hz, 1H), 4.92 (d, *J* = 13.3 Hz, 1H), 4.76 (d, *J* = 13.3 Hz, 1H), 4.67 (s, 2H), 4.27 (ddd, *J* = 9.4, 6.1, 4.9 Hz, 1H), 4.17 (ddd, *J* = 5.8, 5.8, 5.7 Hz, 1H), 4.01 (septet, *J* = 6.2 Hz, 1H), 3.87 (dd, *J* = 5.9, 5.9 Hz, 1H), 3.65 (d, *J* = 5.8 Hz, 2H), 2.64 (d, *J* = 9.4 Hz, 1H), 1.19 (d, *J* = 6.0 Hz, 3H), 1.18 (d, *J* = 6.0 Hz, 3H). ¹³C NMR (125 MHz, CDCl₃) δ 147.8 (2C), 145.9 (2C), 128.1, 128.0, 124.0 (2C), 100.4, 85.8, 80.5, 77.9, 73.1, 72.4, 71.5, 70.8, 23.9, 22.2. MS (TOF ES⁺) *m/z* calcd C₂₂H₃₀N₃O₉ [M + NH₄⁺], 480.19820; found, 480.19401.

Isopropyl 2-O-(Trifluoromethylsulfonyl)-3,5-di-O-(4-nitrobenzyl)-β-D-arabinofuranoside (8). To a solution of 0.025 g (0.054 mmol) of the ribofuranoside (**7**) and 0.066 mL (0.81 mmol) of pyridine in 1 mL of dry dichloromethane was added triflic anhydride (0.11 mL of 1 M solution in dichloromethane) at 0 °C. The reaction was stirred under argon in an ice bath for 30 min, then quenched with 5 mL of a 1:1 mixture of ice and saturated NaHCO₃ solution. The mixture was extracted with 2 × 10 mL of dichloromethane, the combined organic layer was dried over Na₂SO₄ and reduced under high vacuum at room temperature. To this was added 5 mL of *n*-heptane, and the resulting suspension was coevaporated in high vacuum at room temperature. The crude triflate (**10**) was obtained (31 mg, 97%) (HPLC *t*_R = 5.30). **8**: ¹H NMR (300 MHz, CDCl₃) δ 8.23 (d, *J* = 9.0 Hz, 2H), 8.19 (d, *J* = 9.0 Hz, 2H), 7.50 (d, *J* = 8.7 Hz, 2H), 7.43 (d, *J* = 9.0 Hz, 2H), 5.2 (d, *J* = 4.5 Hz, 1H), 5.11 (dd, *J* = 6.3, 4.5 Hz, 1H), 4.73 (s, 2H), 4.67 (s, 2H), 4.37 (dd, *J* = 6.0, 5.4 Hz, 1H), 4.20 (ddd, *J* = 6.0, 5.8, 5.4 Hz, 1H), 3.96 (septet, *J* = 6.3 Hz, 1H), 3.72 (dd, *J* = 9.9, 4.5 Hz, 1H), 3.67 (dd, *J* = 9.9, 6.0 Hz, 1H), 1.19 (d, *J* = 6.2 Hz, 3H), 1.17 (d, *J* = 6.2 Hz, 3H). ¹³C NMR (125 MHz, CDCl₃) δ 145.0, 144.3, 134.6, 130.1, 129.0, 128.3, 127.8, 123.8, 98.3, 87.8, 82.4, 78.9, 72.3, 72.1, 71.3, 23.4, 21.5. MS (TOF ES⁺) *m/z* calcd C₂₃H₂₉F₃N₃O₁₁S [M + NH₄⁺], 612.14749; found, 612.14259.

Isopropyl 2-Deoxy-2-fluoro-3,5-di-O-(4-nitrobenzyl)-β-D-ribofuranoside (9). KF (3 mg, 0.05 mmol) and Kryptofix (19 mg, 0.05 mmol) were azeotropically dried with acetonitrile (3 × 0.3 mL) in a stream of dry nitrogen at 100 °C. To the obtained KF/K2.2.2 complex, 0.03 g (0.05 mmol) of triflate (**8**) was added in 0.2 mL of dry acetonitrile. The reaction vessel was sealed and heated to 154 °C for 30 min. PTLC purification on silica gel with dichloromethane afforded 0.014 g (76%) of **9**: ¹H NMR (300 MHz, CDCl₃) δ 8.21 (d, *J* = 9.0

H₂, 2H), 8.20 (d, *J* = 9.0 Hz, 2H), 7.53 (d, *J* = 8.7 Hz, 2H), 7.52 (d, *J* = 9.0 Hz, 2H), 5.27 (d, *J* = 11.1 Hz, 1H), 4.92 (dd, *J* = 53.5, 3.6 Hz, 1H), 4.81 (d, *J* = 12.9 Hz, 1H), 4.70 (s, 2H), 4.69 (d, *J* = 12.9 Hz, 1H), 4.36 (ddd, *J* = 7.6, 5.7, 3.6 Hz, 1H), 4.20 (ddd, *J* = 23.9, 7.8, 3.6 Hz, 1H), 3.98 (septet, *J* = 6.3 Hz, 1H), 3.78 (dd, *J* = 10.7, 3.6 Hz, 1H), 3.69 (dd, *J* = 10.7, 5.7 Hz, 1H), 1.15 (d, *J* = 6.5 Hz, 3H), 1.13 (d, *J* = 6.5 Hz, 3H). ¹³C NMR (125 MHz, CDCl₃) δ 147.9, 147.8, 146.0, 145.1, 128.1, 127.9, 124.0, 123.96, 103.3 (d, *J* = 29.3 Hz, 1C), 92.5 (d, *J* = 185.3 Hz, 1C), 79.8, 79.1 (d, *J* = 15.6 Hz, 1C), 72.4, 72.2, 71.6, 70.4, 23.7, 21.6. ¹⁹F NMR (282 MHz, CDCl₃) δ -208.58 (ddd, *J* = 53.6, 23.9, 11.4 Hz). MS (TOF ES⁺) *m/z* calcd C₂₂H₂₉FN₃O₈ [M + NH₄⁺], 482.19387; found, 482.18903.

2-DFR (1). The protected fluororibose **9** (0.014 g, 0.03 mmol) was dissolved in 0.1 mL of 90% aqueous formic acid, and 0.03 g of Raney Ni was added. The suspension was heated to 130 °C for 30 min and passed through Amberlite resin (OH⁻ source) washing with 2 mL of MeOH-CH₂Cl₂ (1:9). The washings were purified by column chromatography on silica gel using 5–10% of MeOH in dichloromethane gradient, yielding 4 mg of **1**. The spectroscopic data were in agreement with that in the literature.²⁴

Radiosynthetic Procedures. K₂₂₂/[¹⁸F]F⁻ Complex Formation. All radiochemistry procedures were carried out in a high pressure compact modular radiosynthesizer.²⁹ No-carrier-added [¹⁸F]-fluoride was produced in an RDS-111 cyclotron (UCLA, biomedical cyclotron) by the nuclear reaction (p,n) of ¹⁸O-enriched water ([¹⁸O]H₂O, 98% isotopic purity, Rotem, Inc.) in a 1 mL silver target (11 MeV beam). [¹⁸F]F⁻ (3700–9250 MBq) was captured and eluted from a QMA cartridge in K₂CO₃ (0.4 mL; 0.605 mM) into a reaction vessel containing Kryptofix 222 (K₂₂₂; 13 mg, 34.58 μmol) dissolved in CH₃CN (0.7 mL). The mixture was heated to 120 °C in an oil bath to complete dryness and anhydrous acetonitrile (0.5 mL) was added and azeotropically evaporated 4 times to remove water and to form the K₂₂₂/[¹⁸F]F⁻ complex.

1-Isopropyl-2-fluoro-3,5-di-O-(4-nitrobenzyl)-β-D-[¹⁸F]-ribofuranoside ([¹⁸F]-9). To the K₂₂₂/[¹⁸F]F⁻ complex, triflate (**8**) (10 mg, 0.016 mmol), dissolved in acetonitrile (500 μL), was added and heated in an oil bath (154 °C; 30 min). The reaction mixture was loaded onto a silica Sep-pak cartridge and eluted with ethyl acetate (2 mL). The compound was heated to dryness in an oil bath (100 °C) under nitrogen.

2-Deoxy-2-[¹⁸F]fluororibose ([¹⁸F]-2-DFR, [¹⁸F]-1). Raney Ni (30 mg) in formic acid (500 μL, 90% in water) was added to [¹⁸F]-**9**, and the reaction mixture was heated (130 °C; 30 min) and filtered through a polypropylene filter (0.45 μm). The filter was rinsed with water (10 mL), and the water and filtrate were passed through the KT-500-2 purification column and a filter (0.22 μm) to yield the final product (**1**). The final product was at a pH of ~6.5 after the purification column and filter and was further neutralized to pH ~7.4 by the addition of 10× PBS to a final concentration of 1× PBS. Total synthesis time from [¹⁸F]F⁻ delivery to the final product was 2.5 h. Purified **1** and [¹⁸F]-**1** were injected into an analytical HPLC coupled to an electrochemical detector (ED50A, Dionex) and a γ detector (Carroll and Ramsey Associates, model 105 S). A CarboPac MA1 column (4 mm × 250 mm) was used with a flow rate of 0.4 mL/min of 150 nM NaOH. Both [¹⁸F]-**1** and **1** eluted with the same retention time. The radiochemical purity of [¹⁸F]-**1** was 95 ± 3%.

Biological Procedures. [¹⁸F]-2-DFR Specific Activity. [¹⁸F]-2-DFR specific activity was measured as previously described except that [¹⁸F]-2-DFR was used in place of [¹⁸F]-DFA.¹² The specific activity of [¹⁸F]-2-DFR was 74 ± 30.9 TBq/mmol.

[¹⁸F]-2-DFR in Vivo Stability. Mice were injected intravenously with ~11.1 MBq of [¹⁸F]-2-DFR. After 1 h, the mice were sacrificed and serum (400 μL) was collected via a cardiac bleed into gel barrier blood collection tubes (Capiject). 25 μL of pure [¹⁸F]-2-DFR or the mouse serum was injected into an HPLC instrument connected to a γ detector.

Mice. Animal studies were performed in accordance with the UCLA Animal Research Committee guidelines. C57Bl/6 mice (female, 8–12 weeks old) were used for the dynamic imaging and

biodistribution studies. C57Bl/6 mice (male, 8–12 weeks old) were used for the acetaminophen studies.

Micro-PET/Computed Tomography (CT) Imaging and Analysis. Mice were anesthetized with 1.5–2% (v/v) isoflurane and immediately injected intravenously with approximately 740 kBq of [¹⁸F]-2-DFR or [¹⁸F]-DFA. [¹⁸F]-DFA was synthesized as previously described.¹² Animals remained anesthetized throughout the imaging experiment. PET scans were performed on an Inveon micro-PET scanner (Siemens), Genisys 4 imager (Sofie Biosciences), and Genisys 8 imager (Sofie Biosciences). CT scans were performed on a micro-CAT II CT scanner (Siemens). For dynamic scans, mice were continuously imaged on a PET scanner from immediate to 2 h postinjection after which the mice were subject to a 10 min CT scan. The PET data were analyzed using the following imaging windows: 2 × 30 s, 4 × 1 min, 5 × 5 min, 9 × 10 min. For static scans, mice were imaged on a CT scanner for 10 min, 50 min postinjection and then immediately imaged on a PET scanner for 10 min. PET images were reconstructed using a OSEM + MAP algorithm. PET/CT images were manually co-registered. Data were imaged and quantified using the AMIDE software as previously described.^{12,30} Figure 3a represents a volume rendering of the PET/CT data. Figure 3f, Figure 5b, Figures 51a, and 52a represent coronal sections.

[¹⁸F]-2-DFR ex Vivo Biodistribution. [¹⁸F]-2-DFR ex vivo biodistribution experiments were performed as previously described except that [¹⁸F]-2-DFR was used in place of [¹⁸F]-DFA.¹²

[¹⁸F]-2-DFR Whole Body Autoradiography. Mice were anesthetized and injected with 37 MBq of [¹⁸F]-2-DFR. After 1 h, the mice were sacrificed, embedded in a 3% (wt/vol) solution of carboxymethylcellulose, and frozen in a dry ice/methanol bath. Digital images and 40 μm sections were cut with a Leica cryostat. Sections were exposed to a Fujifilm imaging plate overnight, and the Fujifilm cassettes were imaged on a Fuji BAS imager.

[¹⁸F]-2-DFR Cell Accumulation Experiments. THLE-2 cells (ATCC; 0.3 × 10⁶ cells/well) were plated in hepatocyte maintenance media (Corning) onto poly-L-lysine-coated 24-well plates and allowed to adhere overnight. 74 kBq of [¹⁸F]-2-DFR and saline or [¹⁸F]-2-DFR and 50 mM ribose were added to each well. The cells were incubated with the [¹⁸F]-2-DFR for 1 h, after which the cells exposed to trypsin, collected, washed 3× with ice-cold hepatocyte maintenance media, and the radioactive accumulation was measured on a γ counter.

[¹⁸F]-2-DFR and Ribose Co-Injection Studies. [¹⁸F]-2-DFR was co-injected with ribose (25 μmoles in 50 μL of 1× PBS) or vehicle (50 μL of 1× PBS). After 50 min, the mice were CT and PET imaged as described above.

[¹⁸F]-2-DFR Transport and Metabolism Studies. [¹⁸F]-2-DFR transport and metabolism studies were performed as previously described except that 2-DFR was used in place of DFA.¹²

Acetaminophen Studies. Overnight fasted mice were injected with acetaminophen (75 mg/mL in sterile saline; 300 mg/kg) or vehicle (sterile saline). At 6 h postinjection, the mice were PET/CT imaged with [¹⁸F]-2-DFR. Following PET/CT imaging, serum (100 μL) was collected via a retroorbital bleed in gel barrier blood collection tubes (Capiject). Alanine aminotransferase and aspartate aminotransferase measurements were performed by the UCLA Division of Laboratory Animal Medicine Diagnostic Lab. Only those mice with elevated alanine aminotransferase and aspartate aminotransferase levels were analyzed as part of the acetaminophen treatment group. PET images were quantified by an individual unaware of the treatment groups.

Statistics. Data are reported as mean ± standard error of the mean. Treatment groups were compared using a Student *t* test in Microsoft Excel. Graphs were created in Microsoft Excel and GraphPad Prism.

■ ASSOCIATED CONTENT

Supporting Information

Figures S1–S3, NMR, HPLC, and MS spectra. The Supporting Information is available free of charge on the ACS Publications website at DOI: 10.1021/acs.jmedchem.5b00569.

AUTHOR INFORMATION

Corresponding Authors

*N.M.E.: e-mail, nevdokim@chem.ucla.edu; phone, (310) 902-8552.

*M.E.J.: e-mail, jung@chem.ucla.edu; phone, (310) 825-7954.

Author Contributions

•N.M.E. and P.M.C. contributed equally.

All authors contributed to the writing of this manuscript. All authors have given approval to the final version of the manuscript.

Notes

The authors declare no competing financial interest.

N.M.E., P.M.C., G.F., O.N.W., and M.E.J. are coauthors on a patent application that includes the [¹⁸F]-2-DFR molecule described in this manuscript.

ACKNOWLEDGMENTS

We thank Dr. David Stout, members of the Crump Institute for Molecular Imaging, and members of the Pasarow Mass Spectrometry Laboratory for their technical assistance and advice. N.M.E. was supported by the Phelps Family Foundation. P.M.C. was supported by the California Institute of Regenerative Medicine Training Grant TG2-01169, the UCLA Scholars in Oncologic Molecular Imaging Program National Cancer Institute Grant R25T CA098010, and the UCLA in Vivo Cellular and Molecular Imaging Center Career Development Award P50 CA086306. T.C. was supported by the University of California Amgen Scholars Program. O.N.W. is an Investigator of the Howard Hughes Medical Institute and is partially supported by the Eli and Edythe Broad Center of Regenerative Medicine and Stem Cell Research. We thank Ralph and Marjorie Crump for a donation made to the University of California, Los Angeles (UCLA) Crump Institute for Molecular Imaging. The National Science Foundation Equipment Grant CHE-1048804 is acknowledged.

ABBREVIATIONS USED

[¹⁸F]-2-DFR, 2-deoxy-2-[¹⁸F]fluororibose; [¹⁸F]-FDG, 2-deoxy-2-[¹⁸F]fluoroglucose; [¹⁸F]-DFA, 2-deoxy-2-[¹⁸F]-fluoroarabinose; PNBn, 4-nitrobenzyl; PRPS, phosphoribosyl pyrophosphate synthetase; RPIA, ribose-5-phosphate isomerase; % ID/g, percent injected dose per gram of tissue

REFERENCES

- (1) Gambhir, S. S. Molecular imaging of cancer with positron emission tomography. *Nat. Rev. Cancer* **2002**, *2*, 683–693.
- (2) Phelps, M. E. Positron emission tomography provides molecular imaging of biological processes. *Proc. Natl. Acad. Sci. U.S.A.* **2000**, *97*, 9226–9233.
- (3) Phelps, M. E.; Mazziotta, J. C. Positron emission tomography: human brain function and biochemistry. *Science* **1985**, *228*, 799–809.
- (4) van Tinteren, H.; Hoekstra, O. S.; Smit, E. F.; van den Bergh, J. H.; Schreurs, A. J.; Stallaert, R. A.; van Velthoven, P. C.; Comans, E. F.; Diepenhorst, F. W.; Verboom, P.; van Mourik, J. C.; Postmus, P. E.; Boers, M.; Teule, G. J. Effectiveness of positron emission tomography in the preoperative assessment of patients with suspected non-small-cell lung cancer: the PLUS multicentre randomised trial. *Lancet* **2002**, *359*, 1388–1393.
- (5) Pio, B. S.; Park, C. K.; Pietras, R.; Hsueh, W. A.; Satyamurthy, N.; Pegram, M. D.; Czernin, J.; Phelps, M. E.; Silverman, D. H. Usefulness of 3'-[F-18]fluoro-3'-deoxythymidine with positron emission tomography in predicting breast cancer response to therapy. *Mol. Imaging Biol.* **2006**, *8*, 36–42.

- (6) Tillisch, J.; Brunken, R.; Marshall, R.; Schwaiger, M.; Mandelkern, M.; Phelps, M.; Schelbert, H. Reversibility of cardiac wall-motion abnormalities predicted by positron tomography. *N. Engl. J. Med.* **1986**, *314*, 884–888.

- (7) Dyson, J. K.; McPherson, S.; Anstee, Q. M. Non-alcoholic fatty liver disease: non-invasive investigation and risk stratification. *J. Clin. Pathol.* **2013**, *66*, 1033–1045.

- (8) Festi, D.; Schiumerini, R.; Marzi, L.; Di Biase, A. R.; Mandolesi, D.; Montrone, L.; Scafoli, E.; Bonato, G.; Marchesini-Reggiani, G.; Colecchia, A. Review article: the diagnosis of non-alcoholic fatty liver disease—availability and accuracy of non-invasive methods. *Aliment. Pharmacol. Ther.* **2013**, *37*, 392–400.

- (9) Malnick, S. D.; Beergabel, M.; Knobler, H. Non-alcoholic fatty liver: a common manifestation of a metabolic disorder. *QJM* **2003**, *96*, 699–709.

- (10) Myers, R. P.; Fong, A.; Shaheen, A. A. Utilization rates, complications and costs of percutaneous liver biopsy: a population-based study including 4275 biopsies. *Liver Int.* **2008**, *28*, 705–712.

- (11) Larson, A. M.; Polson, J.; Fontana, R. J.; Davern, T. J.; Lalani, E.; Hyman, L. S.; Reisch, J. S.; Schiodt, F. V.; Ostapowicz, G.; Shakil, A. O.; Lee, W. M. Acetaminophen-induced acute liver failure: results of a United States multicenter, prospective study. *Hepatology* **2005**, *42*, 1364–1372.

- (12) Clark, P. M.; Flores, G.; Evdokimov, N. M.; McCracken, M. N.; Chai, T.; Nair-Gill, E.; O'Mahony, F.; Beaven, S. W.; Faull, K. F.; Phelps, M. E.; Jung, M. E.; Witte, O. N. Positron emission tomography probe demonstrates a striking concentration of ribose salvage in the liver. *Proc. Natl. Acad. Sci. U.S.A.* **2014**, *111*, E2866–E2874.

- (13) Goncalves, R. P.; Bennett, G. C.; Leblond, C. P. Fate of 3H-ribose in the rat as detected by radioautography. *Anat. Rec.* **1969**, *165*, 543–557.

- (14) Miller, P. W.; Long, N. J.; Vilar, R.; Gee, A. D. Synthesis of ¹¹C, ¹⁸F, ¹⁵O, and ¹³N radiolabels for positron emission tomography. *Angew. Chem., Int. Ed.* **2008**, *47*, 8998–9033.

- (15) Deng, H.; Cobb, S. L.; Gee, A. D.; Lockhart, A.; Martarello, L.; McGlinchey, R. P.; O'Hagan, D.; Omega, M. Fluorinase mediated C-F-18 bond formation, an enzymatic tool for PET labelling. *Chem. Commun.* **2006**, 652–654.

- (16) Li, X. G.; Autio, A.; Ahtinen, H.; Helariutta, K.; Liljenback, H.; Jalkanen, S.; Roivainen, A.; Airaksinen, A. J. Translating the concept of peptide labeling with 5-deoxy-5-[F-18] fluororibose into preclinical practice: F-18-labeling of Siglec-9 peptide for PET imaging of inflammation. *Chem. Commun.* **2013**, *49*, 3682–3684.

- (17) Park, J.; van Koeven, P.; Singh, B.; Gupta, R. S. Identification and characterization of human ribokinase and comparison of its properties with *E. coli* ribokinase and human adenosine kinase. *FEBS Lett.* **2007**, *581*, 3211–3216.

- (18) Furuya, T.; Kuttruff, C. A.; Ritter, T. Carbon-fluorine bond formation. *Curr. Opin. Drug Discovery Dev.* **2008**, *11*, 803–819.

- (19) Huang, X. Y.; Liu, W.; Ren, H.; Neelamegam, R.; Hooker, J. M.; Groves, J. T. Late stage benzylic C-H fluorination with [F-18]fluoride for PET imaging. *J. Am. Chem. Soc.* **2014**, *136*, 6842–6845.

- (20) Liu, W.; Huang, X. Y.; Cheng, M. J.; Nielsen, R. J.; Goddard, W. A.; Groves, J. T. Oxidative aliphatic C-H fluorination with fluoride ion catalyzed by a manganese porphyrin. *Science* **2012**, *337*, 1322–1325.

- (21) Dahlman, O.; Garegg, P. J.; Mayer, H.; Schramek, S. Synthesis of 3-C-hydroxymethylpentoses with the D-ribo-configurations, D-xylo-configurations and L-lyxo-configurations—Identification of the latter with a monosaccharide isolated from phase-I *Coxiella-burnetii* lipopolysaccharide. *Acta Chem. Scand., Ser. B* **1986**, *40*, 15–20.

- (22) Larsen, C. H.; Ridgway, B. H.; Shaw, J. T.; Smith, D. M.; Woerpel, K. A. Stereoselective C-glycosylation reactions of ribose derivatives: Electronic effects of five-membered ring oxocarbenium ions. *J. Am. Chem. Soc.* **2005**, *127*, 10879–10884.

- (23) Lopez, J. C.; Ventura, J.; Uriel, C.; Gomez, A. M.; Fraser-Reid, B. Reaction of 1,2-orthoesters with HF-pyridine: A method for the preparation of partly unprotected glycosyl fluorides and their use in saccharide synthesis. *Org. Lett.* **2009**, *11*, 4128–4131.

(24) Sanderson, P. N.; Sweatman, B. C.; Farrant, R. D.; Lindon, J. C. Assignment of the H-1, F-19, and C-13 NMR spectra of 2-deoxy-2-fluoro-D-ribose and characterisation of the isomeric equilibrium. *Carbohydr. Res.* **1996**, *284*, 51–60.

(25) Berg, J. M.; Tymoczko, J. L.; Stryer, L. *Biochemistry*; W. H. Freeman: New York, 2002.

(26) Larson, A. M. Acetaminophen hepatotoxicity. *Clin. Liver Dis.* **2007**, *11*, 525–548.

(27) Ward, J.; Kanchagar, C.; Veksler-Lublinsky, I.; Lee, R. C.; McGill, M. R.; Jaeschke, H.; Curry, S. C.; Ambros, V. R. Circulating microRNA profiles in human patients with acetaminophen hepatotoxicity or ischemic hepatitis. *Proc. Natl. Acad. Sci. U.S.A.* **2014**, *111*, 12169–12174.

(28) Lenagh-Snow, G. M. J.; Araujo, N.; Jenkinson, S. F.; Rutherford, C.; Nakagawa, S.; Kato, A.; Yu, C. Y.; Weymouth-Wilson, A. C.; Fleet, G. W. J. Inhibition of nonmammalian glycosidases by azetidine iminosugars derived from stable 3,5-di-O-triflates of pentoses. *Org. Lett.* **2011**, *13*, 5834–5837.

(29) Amaraesekera, B.; Marchis, P. D.; Bobinski, K. P.; Radu, C. G.; Czernin, J.; Barrio, J. R.; van Dam, R. M. High-pressure, compact, modular radiosynthesizer for production of positron emitting biomarkers. *Appl. Radiat. Isot.* **2013**, *78*, 88–101.

(30) Loening, A. M.; Gambhir, S. S. AMIDE: A completely free system for medical imaging data analysis. *J. Nucl. Med.* **2001**, *42*, 192P–192P.